nature medicine

Brown adipose tissue activity controls triglyceride clearance

Alexander Bartelt[1], Oliver T Bruns[2], Rudolph Reimer[2], Heinz Hohenberg[2], Harald Ittrich[3], Kersten Peldschus[3], Michael G Kaul[3], Ulrich I Tromsdorf[4], Horst Weller[4], Christian Waurisch[5], Alexander Eychmüller[5], Philip L S M Gordts[6], Franz Rinninger[7], Karoline Bruegelmann[1], Barbara Freund[1], Peter Nielsen[1], Martin Merkel[1,8] & Joerg Heeren[1]

Brown adipose tissue (BAT) burns fatty acids for heat production to defend the body against cold[1,2] and has recently been shown to be present in humans[3–5]. Triglyceride-rich lipoproteins (TRLs) transport lipids in the bloodstream, where the fatty acid moieties are liberated by the action of lipoprotein lipase (LPL)[6]. Peripheral organs such as muscle and adipose tissue take up the fatty acids, whereas the remaining cholesterol-rich remnant particles are cleared by the liver[6]. Elevated plasma triglyceride concentrations and prolonged circulation of cholesterol-rich remnants, especially in diabetic dyslipidemia, are risk factors for cardiovascular disease[7–11]. However, the precise biological role of BAT for TRL clearance remains unclear. Here we show that increased BAT activity induced by short-term cold exposure controls TRL metabolism in mice. Cold exposure drastically accelerated plasma clearance of triglycerides as a result of increased uptake into BAT, a process crucially dependent on local LPL activity and transmembrane receptor CD36. In pathophysiological settings, cold exposure corrected hyperlipidemia and improved deleterious effects of insulin resistance. In conclusion, BAT activity controls vascular lipoprotein homeostasis by inducing a metabolic program that boosts TRL turnover and channels lipids into BAT. Activation of BAT might be a therapeutic approach to reduce elevated triglyceride concentrations and combat obesity in humans.

Although white adipose tissue is a specialized lipid storage organ for excess calories, BAT contains large amounts of mitochondria to dissipate chemical energy. Upon cold-stimulated activation by nervous input, BAT increases its energy demand and burns carbohydrates and lipids to produce heat using uncoupling protein-1 (UCP1), a protein that uncouples electron transport from ATP production[1]. Recent evidence that BAT is also present in humans[2–5] has led to a growing interest in understanding BAT development and physiology. However, the role of lipoproteins for fuel delivery to BAT remained unknown. To determine whether cold exposure alters the lipoprotein profile, we analyzed plasma from FVB wild-type mice kept at 22 °C (control mice) or at 4 °C in a cold room (cold mice) by fast-performance liquid chromatography (FPLC). TRL-triglyceride concentrations were markedly reduced after 4 h and 24 h (**Fig. 1a**), indicating that cold exposure lowers triglyceride levels efficiently. HDL-cholesterol abundance, however, was slightly increased (**Fig. 1b**), which is probably explained by an increase of TRL-derived HDL precursors[12].

After a fatty meal, triglyceride-rich chylomicrons transport dietary lipids, but it is unclear whether BAT is involved in their processing. Therefore we performed an oral fat tolerance test with olive oil mixed with ^{3}H-triolein in wild-type FVB mice. In control mice, triglyceride concentrations rose with a peak at 2 h and a subsequent decline (**Fig. 1c**), as expected[6,13]. In cold mice, triglyceride levels remained persistently low during the postprandial phase (**Fig. 1c**). The lipoprotein profile (**Fig. 1d** and **Supplementary Fig. 1**) confirmed the presence of chylomicrons in control mice, whereas they were absent in cold mice. The corresponding ^{3}H-radioactivity profile resembled the curve for triglycerides in control mice, whereas in cold mice plasma ^{3}H-radioactivity steadily rose (**Supplementary Fig. 2**). The latter can be explained by the occurrence of small-molecule fatty acid degradation products in the blood (**Supplementary Fig. 3**). Organ distribution of ^{3}H-triolein–derived radioactivity 2 h after gavage (**Fig. 1e** and **Supplementary Fig. 4**) revealed a selective increase in organ uptake of fatty acids into BAT. In cold mice the total contribution of BAT uptake was higher than for muscle, which also participates in heat production in response to acute cold by shivering thermogenesis[1]. As the production rates of hepatic (**Supplementary Fig. 5**) and intestinal TRLs (**Supplementary Fig. 6**) were unaltered by cold exposure, the increase in specific uptake of TRL-lipids into different BAT depots suggests an accelerated clearance of postprandial TRLs in cold mice.

To investigate the clearance and kinetics in more detail, we embedded both ^{3}H-triolein and hydrophobic ^{59}Fe-superparamagnetic iron oxide (SPIO) nanocrystals into the core of TRL particles. These particles allowed us to follow lipoprotein and fatty acid uptake simultaneously, because upon LPL-mediated lipolysis, ^{3}H-oleate was released, whereas hydrophobic ^{59}Fe-SPIO nanocrystals remained within the TRL cores (**Supplementary Figs. 7** and **8**). Clearance of both TRL-derived ^{59}Fe-SPIO

[1]Institute of Biochemistry and Molecular Biology II: Molecular Cell Biology, University Medical Center Hamburg-Eppendorf, Hamburg, Germany. [2]Department of Electron Microscopy and Micro Technology, Heinrich-Pette Institute, Hamburg, Germany. [3]Department of Diagnostic and Interventional Radiology, University Medical Center Hamburg-Eppendorf, Hamburg, Germany. [4]Institute of Physical Chemistry, University of Hamburg, Hamburg, Germany. [5]Physical Chemistry, Technical University Dresden, Dresden, Germany. [6]Department of Human Genetics, University of Leuven, Leuven, Belgium. [7]III. Department of Internal Medicine, University Medical Center Hamburg-Eppendorf, Hamburg, Germany. [8]Asklepios Clinic St. Georg, Department of Internal Medicine, Hamburg, Germany. Correspondence should be addressed to A.B. (abartelt@uke.uni-hamburg.de) or J.H. (heeren@uke.uni-hamburg.de).

Received 12 October 2010; accepted 22 December 2010; published online 23 January 2011; doi:10.1038/nm.2297

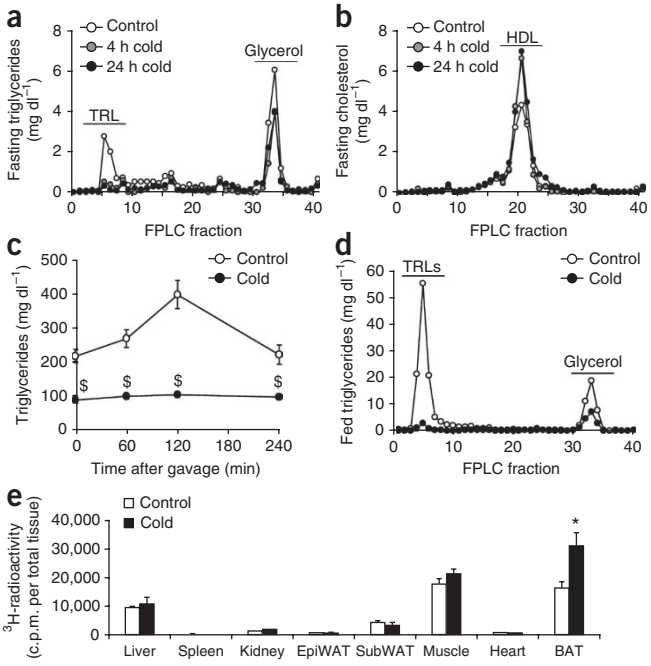

Figure 1 Cold exposure modulates fasting and postprandial triglyceride-rich lipoprotein levels. (**a**,**b**) Triglyceride (**a**) and cholesterol (**b**) FPLC profiles of pooled plasma from fasted FVB mice after 4 h and 24 h cold exposure at 4 °C. (**c**) Plasma triglycerides during an oral fat tolerance test in control and cold-exposed FVB mice. (**d**) FPLC lipoprotein profiling in control and cold-exposed FVB mice 2 h after an oral fat load. (**e**) Organ distribution of triolein-derived ^{3}H-radioactivity in control and cold-exposed FVB mice 2 h after gavage. EpiWAT, epididymal white adipose tissue; SubWAT, subcutaneous white adipose tissue. Mean values ± s.e.m. with $n = 12$ in **c** and $n = 4$ in **e**. $^{*}P < 0.05$; $\$P < 0.001$.

(**Fig. 2a**) and ^{3}H-triolein (**Fig. 2b**) was significantly faster in cold mice compared to control mice. The organ distributions of ^{3}H-triolein and ^{59}Fe-SPIO indicated that the accelerated clearance was mediated by an approximately tenfold increase in specific uptake into BAT in cold mice versus control mice (**Fig. 2c**,**d** and **Supplementary Fig. 9**). Total amounts of ^{3}H-triolein and ^{59}Fe-SPIO uptake in BAT in cold mice were comparable to total liver uptake in both cold mice and control mice, whereas the contribution of other tissues to uptake was small in both sets of mice (**Fig. 2c**,**d**). We confirmed these findings with TRL particles which were double-labeled with a conventional, nonreleasable core lipid, ^{3}H-cholesterol ethers and ^{14}C-triolein (**Supplementary Figs. 10** and **11**). In cold-exposed mice, the uptake of both lipid labels was substantially increased into BAT, whereas we observed reduced hepatic TRL uptake, indicating that cold exposure shifted the clearance of lipoproteins from liver to BAT. Notably, uptake into subcutaneous white adipose tissue was also increased (**Fig. 2c**,**d**), which can be explained by the presence and activation of brown adipocytes after cold exposure (**Supplementary Fig. 12**).

We used hydrophobic SPIO nanocrystals, which accelerate spin-spin relaxations, embedded into TRL cores to follow lipoprotein uptake into the liver by dynamic magnetic resonance imaging (MRI)[14]. Irrespective of BAT activity, we observed uptake into the liver of control and cold-exposed mice (**Fig. 2e**). However, cold exposure markedly increased the negative contrast of several BAT depots, indicative of increased TRL presence (**Fig. 2e**,**f**, **Supplementary Fig. 13** and **Supplementary Video 1**). We observed a pronounced negative contrast in BAT even 1 week after injection (**Fig. 2g**), suggesting uptake of the entire SPIO-labeled lipoprotein particle.

Intravital microscopy enables the study of physiologic processes *in vivo* on a cellular level. We visualized the vascular circulation and structure of interscapular BAT in real time. In cold-exposed mice, BAT-mediated processing of TRLs labeled with hydrophobic fluorescent nanocrystals (QD-TRLs) revealed a rapid attachment to the endothelium, which was followed by QD-TRL internalization (**Fig. 2h** and **Supplementary Video 2**). Cryoelectron microscopy studies showed that in cold mice SPIOs were detectable underneath capillaries of BAT 30 min after injection (**Fig. 2i**), indicating TRL particle internalization.

It has been shown that TRL lipolysis products cause a decrease in endothelial barrier function[15]. By injection of Evans blue dye or ^{125}I-labeled albumin with or without inhibiting lipolysis, we found that endothelial permeability in BAT is increased upon cold exposure and that this process is dependent on simultaneous lipolysis (**Supplementary Fig. 14**). These findings indicate that cold exposure–induced increase in lipoprotein turnover remodels endothelial permeability thereby allowing an increased internalization of TRLs into BAT. Taken together, activated BAT accelerates plasma TRL turnover and is a major target organ for TRL uptake.

To gain further mechanistic insight into BAT-mediated TRL processing, we studied turnover and organ uptake of radiolabeled TRLs in transgenic mouse models that have defective function of proteins key for lipolysis (apolipoprotein AV (apoAV))[13,16] and particle uptake (apolipoprotein E (apoE), low-density lipoprotein receptor (LDLR), low-density lipoprotein receptor–related protein-1 (LRP1))[17–21], but none of them showed a reduced uptake of radiolabeled TRLs into BAT (**Supplementary Fig. 15**); moreover, uptake was increased in apoE- and apoAV-deficient mice, probably owing to impaired liver uptake. To assess whether the canonical LPL pathway is involved in uptake of TRLs into BAT, we inhibited LPL activity by injecting the specific inhibitor tetrahydrolipstatin[22]. Local LPL activity in BAT is required for the uptake of TRLs as tetrahydrolipstatin pretreatment abolished uptake of both ^{59}Fe-SPIO and ^{3}H-triolein into BAT of cold mice (**Fig. 3a**,**b**). In addition, release of LPL from the endothelium by heparin pretreatment also blocked uptake of ^{3}H-triolein and ^{59}Fe-SPIO into BAT (**Fig. 3a**,**b**). It is noteworthy that heparin leads to transient maximized LPL activity in the blood stream[23]; however, the amount of fatty acids internalized into BAT under these conditions was very low compared to mock-treated mice (**Fig. 3a**,**b**). These results indicate that local LPL activity in BAT drives lipolysis and is required for fatty acid as well as for TRL particle uptake into BAT. In line with the observation that cold exposure lowers postprandial triglyceride levels (**Fig. 1c**), mock-treated cold mice showed no increase in plasma triglycerides after lipid gavage (**Fig. 3c**). In contrast, tetrahydrolipstatin-treated cold mice showed a significant postprandial triglyceride response (**Fig. 3c**), supporting a role of LPL for triglyceride clearance in cold mice. Intravital confocal imaging showed that, after initial TRL binding to the vascular wall, fluorescent-labeled TRLs can be released by heparin (**Supplementary Video 3**). However, time-delayed heparin injection had no influence on already internalized TRL particles but did block binding of a second bolus of TRLs (**Supplementary Videos 4** and **5**). Taken together, these data indicate that uptake of TRLs into BAT comprises heparin-sensitive initial binding to the vessel wall and subsequent internalization of particles in an LPL-dependent manner.

To find candidates that could influence TRL or fatty acid uptake, we analyzed the gene expression profile of BAT from C57BL/6J mice after cold exposure by real-time PCR (**Fig. 3d**). Among the regulated genes were those encoding known factors for thermogenesis (*Ppargc1a*

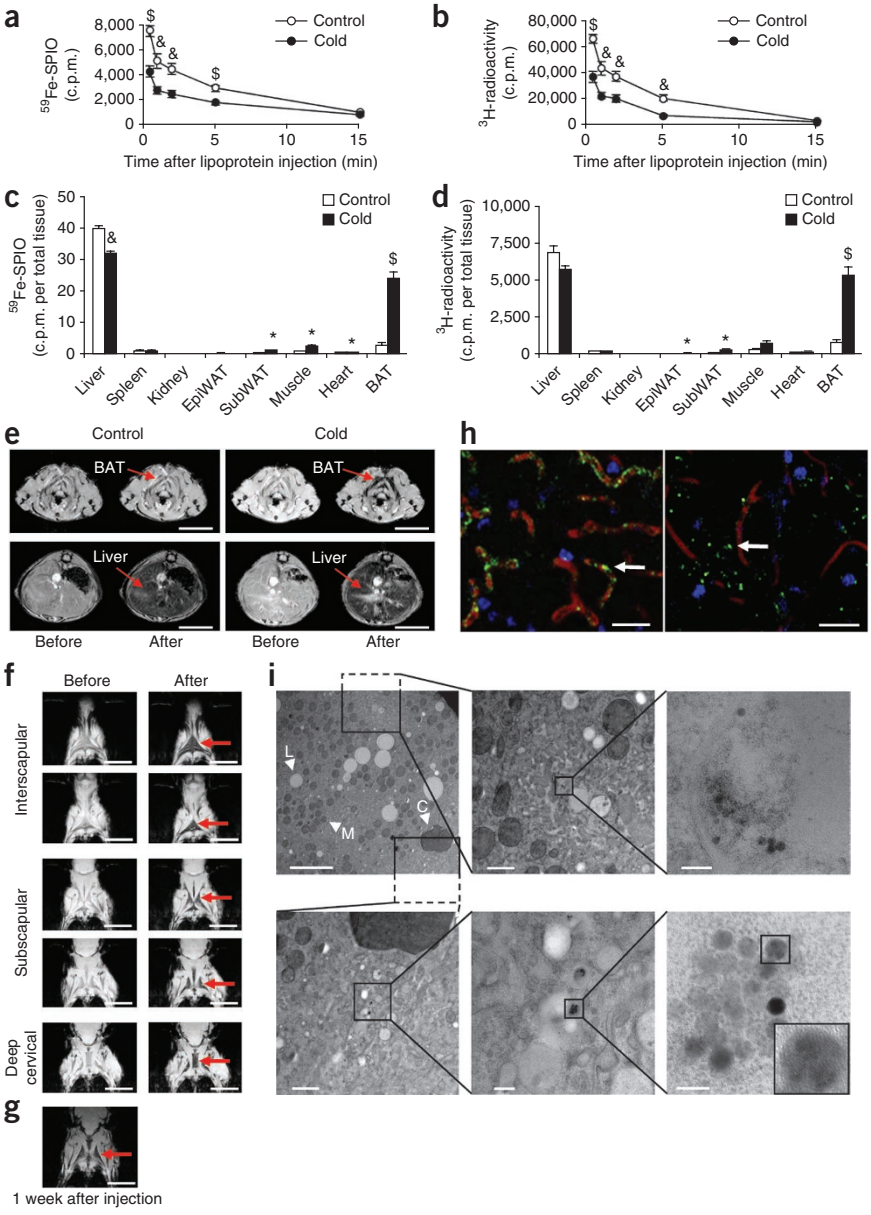

Figure 2 Activated BAT is a central target organ for TRL uptake. (**a**,**b**) Plasma clearance of ^{59}Fe-SPIO (**a**) and ^{3}H-triolein-labeled TRLs (**b**) in control and cold-exposed C57BL/6 mice. (**c**,**d**) Organ distribution of ^{59}Fe-SPIO (**c**) and triolein-derived ^{3}H-radioactivity (**d**) 15 min after intravenous injection. Mean values ± s.e.m. with $n \geq 5$. (**e**) Representative transversal MRIs of a control and a cold-exposed wild-type FVB mouse before and approximately 10 min after injection of SPIO-labeled TRLs. Arrows in the top images point to BAT, whereas arrows in the bottom images indicate the liver. Scale bar, 1 cm. (**f**,**g**) Coronal MRIs of a representative cold mouse before and 10 min after (**f**) and 1 week after (**g**) injection of SPIO-TRLs with identical MRI settings. (**h**) Representative intravital confocal microscopy images of dissected BAT in a live cold-exposed FVB mouse 2 min (left) and 30 min (right) after QD-TRL (green) injection (arrows indicate QD-TRLs). FITC-dextran (red) to stain blood vessels and DAPI (blue) to label nuclei. Scale bar, 25 µm. (**i**) Representative transmission electron microscopy pictures of high-pressure frozen BAT samples from a SPIO-TRL–injected, cold-exposed FVB mouse. L, lipid droplet; M, mitochondrium; C, capillary. Top left scale bar, 5 µm; top middle scale bar, 1 µm; top right scale bar, 0.05 µm; bottom left scale bar, 1 µm; bottom middle scale bar, 0.05 µm; bottom right scale bar, 0.02 µm. *$P < 0.05$; &$P < 0.01$; \$$P < 0.001$.

(encoding peroxisome proliferator–activated receptor γ, coactivator 1α), *Ucp1* and *Dio2* (type II iodothyronine deiodinase))[1], factors involved in lipoprotein metabolism (*Apoe*, *Lrp1*, *Lpl*, *Gpihbp1* (GPI-anchored HDL-binding protein-1), *Angptl4* (angiopoietin-like 4) and *Ldlr*)[6,24–27] and factors important for fatty acid uptake (*Slc27a1, Slc27a3, Slc27a4* and *Cd36*)[28,29].The expression of the gene coding for the adipocyte master transcription factor peroxisome proliferator-activated receptor-γ (*Pparg*) was not influenced.

Vascular endothelial growth factor-B (VEGF-B) has recently been described to facilitate endothelial fatty acid uptake by a specific stimulatory effect on *Slc27a3* and *Slc27a4* expression[28]. After cold exposure we observed that in BAT of wild-type mice the expression of *Cd36*, a gene coding for a transmembrane lipid and lipoprotein receptor, was significantly increased, whereas other fatty acid transporters and *Vegfb* had a rather decreased expression (**Fig. 3e**). Furthermore, compared to *Slc27a3* and *Slc27a4*, mRNA copy numbers of *Cd36* were the highest (**Fig. 3e**), which prompted us to analyze TRL metabolism after cold exposure in *Cd36*$^{-/-}$ mice. A crucial role of CD36 in the thermogenic process was evident because approximately 60% of *Cd36*$^{-/-}$ mice died during the 24 h cold exposure (data not shown). Therefore, we reduced the exposure time to 12 h, leading to a drastically reduced body temperature in *Cd36*$^{-/-}$ mice (**Supplementary Fig. 16**) associated with low locomotor activity and noticeable shivering (**Supplementary Videos 6** and **7**). After 12 h recovery at 22 °C, *Cd36*$^{-/-}$ mice were indistinguishable from wild-type mice (**Supplementary Video 8**). The increase in free fatty acid concentrations in plasma of *Cd36*$^{-/-}$ mice, which was even more pronounced after cold exposure, underlines the major role of this receptor in lipid uptake (**Supplementary Table 1**). FPLC analyses showed that this phenotype correlated not only with a slower turnover of ^{3}H-triolein-TRLs but also with delayed clearance of ^{3}H-oleate bound to albumin compared to cold wild-type mice (**Fig. 3f** and **Supplementary Fig. 17**). Consequently, we observed a significant reduction in ^{59}Fe-SPIO- as well as ^{3}H-triolein-TRL uptake into BAT (**Fig. 3g**,**h**), indicating that CD36 is key for both fatty acid and lipoprotein particle uptake in cold mice. We conclude that CD36 is a major regulator of TRL metabolism and TRL-derived fatty acid uptake into BAT.

Given the high impact of BAT on TRL turnover, we investigated whether BAT activation is also able to lower plasma triglyceride abundance in *Apoa5*$^{-/-}$ mice. This model of severe hyperlipidemia shows an impaired lipolytic TRL processing[13,16]. In these mice, cold exposure corrected plasma lipid concentrations within hours, and TRL-triglyceride as well as TRL-cholesterol levels declined to values comparable to fasted wild-type mice (**Fig. 4a–c**). Thus, we

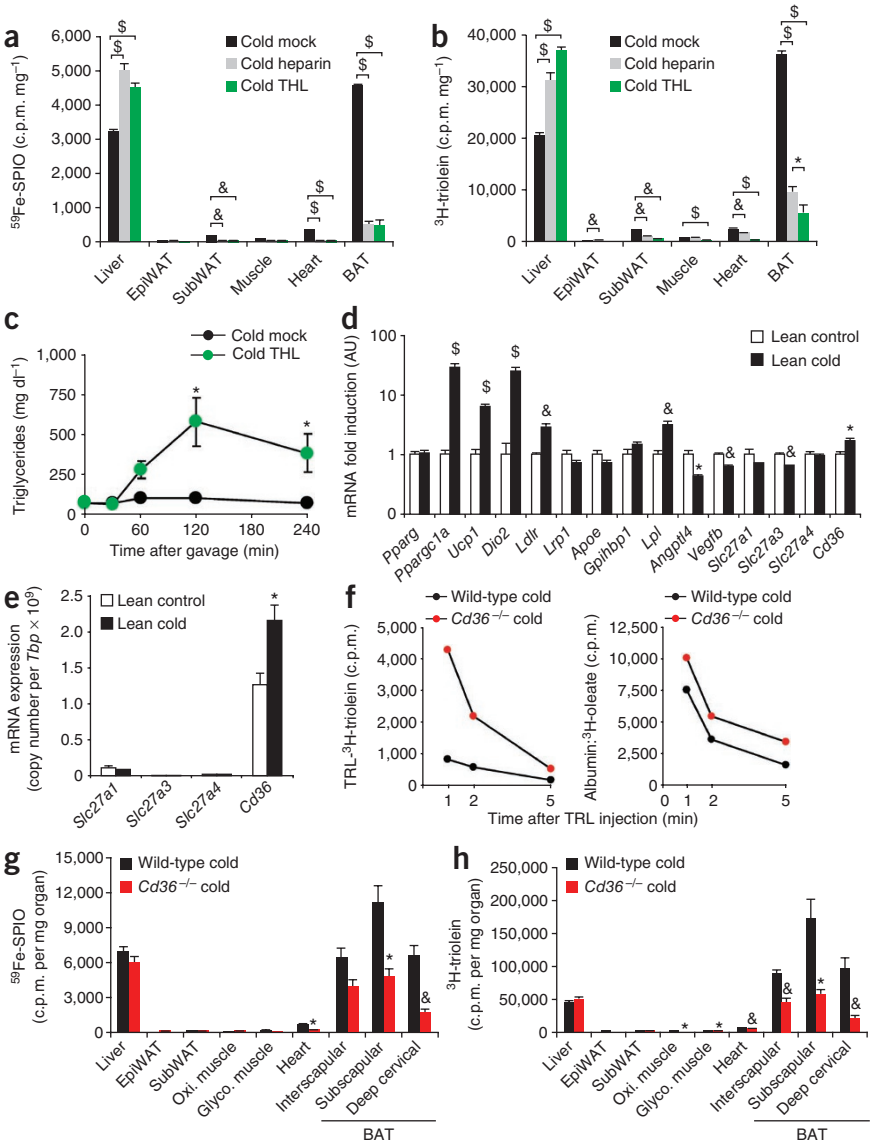

Figure 3 LPL and CD36 drive TRL clearance into BAT. (**a**,**b**) Organ distribution of ^{59}Fe-SPIO (**a**) and triolein-derived ^{3}H (**b**) radioactivity 15 min after intravenous injection in cold FVB mice that were preinjected with tetrahydrolipstatin (THL) to inhibit LPL activity or with heparin to release LPL into circulation, respectively. Mean values ± s.e.m. with $n \geq 5$. (**c**) Oral fat tolerance test in cold FVB mice pretreated with THL. Mean values ± s.e.m. with $n = 5$. (**d**) Relative mRNA expression in C57BL/6J BAT of several genes. The values for the lean control samples were arbitrarily set to 1 for each gene examined. AU, arbitrary units. (**e**) Determination of *Cd36* and other fatty acid transporters mRNA copy numbers normalized to the housekeeping TATA-binding protein (*Tbp*) mRNA by TaqMan. (**f**) Consecutive FPLC analysis of TRL-^{3}H-triolein and albumin-^{3}H-oleate in cold-exposed wild-type and *Cd36*$^{-/-}$ littermates. (**g**,**h**) Organ distribution of ^{59}Fe-SPIO (**g**) and triolein-derived ^{3}H (**h**) radioactivity 15 min after intravenous injection of radiolabeled TRLs into *Cd36*$^{-/-}$ and wild-type littermates. Mean values ± s.e.m. with $n \geq 6$. $^{*}P < 0.05$; &$P < 0.01$; \$$P < 0.001$.

conclude that modulation of BAT activity can correct hyperlipidemia.

To further delineate the biological role of BAT in a pathophysiological state, we analyzed TRL metabolism in a well-established model of diet-induced obesity and insulin resistance (**Supplementary Table 2**)[30]. Brown adipocytes of obese mice appeared hypertrophic compared to lean controls, as determined by environmental scanning electron microscopy (**Fig. 4d**). Notably, after cold-induced lipolysis, lipid droplets in brown adipocytes from lean and obese mice shrank to a similar extent, which was also emphasized by the brownish reappearance of interscapular BAT (**Fig. 4e**). The expression profile of cold-modulated genes was similar in lean and obese mice (**Supplementary Fig. 18**), and, consequently, there was no significant correlation between body weight and weight loss (**Supplementary Fig. 19**). Next we investigated whether glucose and TRL metabolism are influenced by BAT in this model of obesity. This was of special interest to us, as it has been suggested that in humans body fat mass inversely correlates with BAT activity, as determined by positron emission tomography–computed tomography with radioactive glucose tracers[5,31,32]. However, it has so far remained unclear whether uptake of glucose, lipid or both into BAT is influenced by insulin or insulin resistance[2,33,34]. As expected, compared to lean controls, a combined oral glucose and fat tolerance test showed an impaired glucose tolerance in control obese mice, which was normalized upon cold exposure (**Supplementary Fig. 20**). Correspondingly, uptakes of ^{14}C-deoxyglucose (**Fig. 4f** and **Supplementary Fig. 21**) and ^{3}H-triolein (**Fig. 4g** and **Supplementary Fig. 22**) were significantly increased into BAT of both lean and obese mice. The stimulated glucose uptake might be explained by increased expression of the glucose transporters *Slc2a1* (*Glut1*) and *Slc2a4* (*Glut4*) in BAT and heart (**Supplementary Fig. 23**). In obese mice, glucose uptake into BAT and heart was higher than in lean mice under cold conditions, which might be explained by improved local insulin sensitivity in cold mice[33] (**Supplementary Fig. 24**). Furthermore, TRL clearance was accelerated in obese mice compared to lean controls under control conditions (**Fig. 4h**), even when corrected for body weight (**Supplementary Fig. 25**). Accordingly, we observed a similar uptake of TRLs into BAT before and after activation in lean and obese mice when corrected for weights of dissected organs (**Fig. 4i** and **Supplementary Fig. 25**), confirming that uptake of TRLs into BAT is independent of insulin levels and insulin resistance. In FVB mice, heart uptake of radiolabeled TRLs increased after cold exposure (**Supplementary Fig. 9**), whereas it decreased in C57BL/6J mice (**Fig. 4i** and **Supplementary Figs. 10c**,**d** and **25d**). Thus, the difference in heart uptake is a reproducible, mouse strain-specific observation.

In summary, we show that after short-term cold exposure BAT is a master regulator of TRL clearance and blood lipid abundance. Fatty acids are efficiently channeled into BAT due to a metabolic program that boosts TRL uptake into BAT. This process is associated with increased endothelial permeability for lipoproteins and is crucially dependent on LPL and CD36. BAT activation is able to correct hyperlipidemia and improves the deleterious effects of obesity, despite insulin resistance. Moreover, we provide a noninvasive method to measure BAT activity

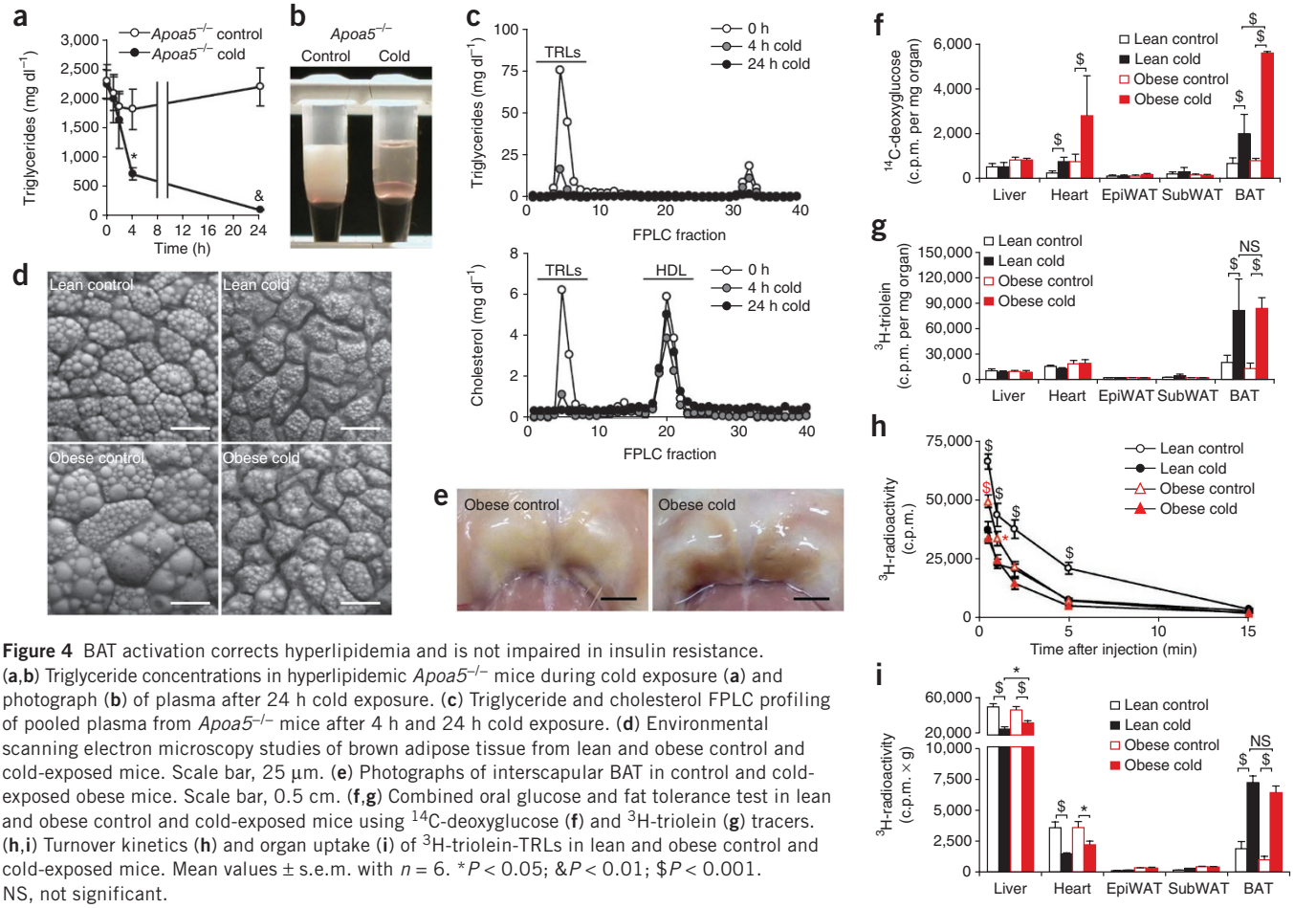

Figure 4 BAT activation corrects hyperlipidemia and is not impaired in insulin resistance. (**a**,**b**) Triglyceride concentrations in hyperlipidemic *Apoa5*$^{-/-}$ mice during cold exposure (**a**) and photograph (**b**) of plasma after 24 h cold exposure. (**c**) Triglyceride and cholesterol FPLC profiling of pooled plasma from *Apoa5*$^{-/-}$ mice after 4 h and 24 h cold exposure. (**d**) Environmental scanning electron microscopy studies of brown adipose tissue from lean and obese control and cold-exposed mice. Scale bar, 25 µm. (**e**) Photographs of interscapular BAT in control and cold-exposed obese mice. Scale bar, 0.5 cm. (**f**,**g**) Combined oral glucose and fat tolerance test in lean and obese control and cold-exposed mice using ^{14}C-deoxyglucose (**f**) and ^{3}H-triolein (**g**) tracers. (**h**,**i**) Turnover kinetics (**h**) and organ uptake (**i**) of ^{3}H-triolein-TRLs in lean and obese control and cold-exposed mice. Mean values ± s.e.m. with $n = 6$. *$P < 0.05$; &$P < 0.01$; \$$P < 0.001$. NS, not significant.

via MRI using nanocrystals embedded into the lipoprotein core. In principle, given the low toxicity of iron-based nanocrystals, this technology is adaptable to a clinical setting and might be a key tool to assess activity of human brown adipose tissue, a future target for therapeutic intervention of obesity and elevated blood lipids.

METHODS

Methods and any associated references are available in the online version of the paper at http://www.nature.com/naturemedicine/.

Note: Supplementary information is available on the Nature Medicine website.

ACKNOWLEDGMENTS

We thank S. Ehret, B. Henkel, E.-M. Azizi, W. Tauscher, C. Edeling, M. Warmer and M. Holthaus for excellent technical assistance. We thank U. Beisiegel for support and critical reading of the manuscript. We thank G. Adam for helpful discussions and support. We thank L. Scheja for helpful discussions and expert technical advice. We are grateful to K.J. Moore (New York University), A. Roebroeck (Katholieke Universiteit Leuven), E.M. Rubin (University of California–Berkeley) and L.A. Pennacchio (University of California–Berkeley) for providing transgenic mouse models. A.B. is a fellow of the Ernst Schering Foundation and is supported by the Graduiertenkolleg der Deutschen Forschungsgemeinschaft 1459. This work was supported by the Landesexzellenzinitiative Hamburg, by Norgenta and by grants from the Deutsche Forschungsgemeinschaft to J.H. and M.M. (ME1507) and A.E. (Schwerpunktprogramm 1313), from the Institute for the Promotion of Innovation through Science and Technology in Flanders to P.L.S.M.G. and from the Bundesministerium für Bildung und Forschung for the Tailored Magnetic Nanoparticles for Cancer Targeting project (TOMCAT, 01 EZ 0824) to H.H., H.I. and P.N. Intravital imaging was performed in collaboration with the Nikon-Applikationszentrum Norddeutschland (Nikon GmbH) at the Heinrich-Pette-Institute.

AUTHOR CONTRIBUTIONS

A.B. and J.H. designed the study, were involved in all aspects of the experiments and co-wrote the manuscript. O.T.B., R.R. and H.H. were responsible for electron microscopy and intravital imaging. H.I., K.P., O.T.B. and M.G.K. were responsible for MRI measurements. C.W., A.E., U.I.T., H.W., B.F. and P.N. were responsible for design and preparation of hydrophobic QD and SPIO, respectively. O.T.B., P.L.S.M.G., F.R., K.B., B.F., P.N. and M.M. were involved in turnover studies. All authors discussed the results and commented on the manuscript.

COMPETING FINANCIAL INTERESTS

The authors declare no competing financial interests.

Published online at http://www.nature.com/naturemedicine/.
Reprints and permissions information is available online at http://npg.nature.com/reprintsandpermissions/.

1. Cannon, B. & Nedergaard, J. Brown adipose tissue: function and physiological significance. *Physiol. Rev.* **84**, 277–359 (2004).
2. Enerbäck, S. Human brown adipose tissue. *Cell Metab.* **11**, 248–252 (2010).
3. Cypess, A.M. *et al.* Identification and importance of brown adipose tissue in adult humans. *N. Engl. J. Med.* **360**, 1509–1517 (2009).
4. Virtanen, K.A. *et al.* Functional brown adipose tissue in healthy adults. *N. Engl. J. Med.* **360**, 1518–1525 (2009).
5. van Marken Lichtenbelt, W.D. *et al.* Cold-activated brown adipose tissue in healthy men. *N. Engl. J. Med.* **360**, 1500–1508 (2009).
6. Williams, K.J. Molecular processes that handle—and mishandle—dietary lipids. *J. Clin. Invest.* **118**, 3247–3259 (2008).

7. Hokanson, J.E. & Austin, M.A. Plasma triglyceride level is a risk factor for cardiovascular disease independent of high-density lipoprotein cholesterol level: a meta-analysis of population-based prospective studies. *J. Cardiovasc. Risk* **3**, 213–219 (1996).
8. Austin, M.A. *et al.* Cardiovascular disease mortality in familial forms of hypertriglyceridemia: a 20-year prospective study. *Circulation* **101**, 2777–2782 (2000).
9. Cullen, P. Evidence that triglycerides are an independent coronary heart disease risk factor. *Am. J. Cardiol.* **86**, 943–949 (2000).
10. Mooradian, A.D. Dyslipidemia in type 2 diabetes mellitus. *Nat. Clin. Pract. Endocrinol. Metab.* **5**, 150–159 (2009).
11. Ginsberg, H.N. Insulin resistance and cardiovascular disease. *J. Clin. Invest.* **106**, 453–458 (2000).
12. von Eckardstein, A., Hersberger, M. & Rohrer, L. Current understanding of the metabolism and biological actions of HDL. *Curr. Opin. Clin. Nutr. Metab. Care* **8**, 147–152 (2005).
13. Merkel, M. *et al.* Apolipoprotein AV accelerates plasma hydrolysis of triglyceride-rich lipoproteins by interaction with proteoglycan-bound lipoprotein lipase. *J. Biol. Chem.* **280**, 21553–21560 (2005).
14. Bruns, O.T. *et al.* Real-time magnetic resonance imaging and quantification of lipoprotein metabolism *in vivo* using nanocrystals. *Nat. Nanotechnol.* **4**, 193–201 (2009).
15. Eiselein, L., Wilson, D.W., Lame, M.W. & Rutledge, J.C. Lipolysis products from triglyceride-rich lipoproteins increase endothelial permeability, perturb zonula occludens-1 and F-actin and induce apoptosis. *Am. J. Physiol. Heart Circ. Physiol.* **292**, H2745–H2753 (2007).
16. Pennacchio, L.A. *et al.* An apolipoprotein influencing triglycerides in humans and mice revealed by comparative sequencing. *Science* **294**, 169–173 (2001).
17. Zhang, S.H., Reddick, R.L., Piedrahita, J.A. & Maeda, N. Spontaneous hypercholesterolemia and arterial lesions in mice lacking apolipoprotein E. *Science* **258**, 468–471 (1992).
18. Brown, M.S. & Goldstein, J.L. A receptor-mediated pathway for cholesterol homeostasis. *Science* **232**, 34–47 (1986).
19. Rohlmann, A., Gotthardt, M., Hammer, R.E. & Herz, J. Inducible inactivation of hepatic LRP gene by Cre-mediated recombination confirms role of LRP in clearance of chylomicron remnants. *J. Clin. Invest.* **101**, 689–695 (1998).
20. Beisiegel, U., Weber, W., Ihrke, G., Herz, J. & Stanley, K.K. The LDL-receptor-related protein, LRP, is an apolipoprotein E-binding protein. *Nature* **341**, 162–164 (1989).
21. Gordts, P.L. *et al.* Inactivation of the LRP1 intracellular NPxYxxL motif in LDLR-deficient mice enhances postprandial dyslipidemia and atherosclerosis. *Arterioscler. Thromb. Vasc. Biol.* **29**, 1258–1264 (2009).
22. Augustus, A.S., Kako, Y., Yagyu, H. & Goldberg, I.J. Routes of FA delivery to cardiac muscle: modulation of lipoprotein lipolysis alters uptake of TG-derived FA. *Am. J. Physiol. Endocrinol. Metab.* **284**, E331–E339 (2003).
23. Neuger, L. *et al.* Effects of heparin on the uptake of lipoprotein lipase in rat liver. *BMC Physiol.* **4**, 13 (2004).
24. Sukonina, V., Lookene, A., Olivecrona, T. & Olivecrona, G. Angiopoietin-like protein 4 converts lipoprotein lipase to inactive monomers and modulates lipase activity in adipose tissue. *Proc. Natl. Acad. Sci. USA* **103**, 17450–17455 (2006).
25. Moore, K.J. *et al.* Loss of receptor-mediated lipid uptake via scavenger receptor A or CD36 pathways does not ameliorate atherosclerosis in hyperlipidemic mice. *J. Clin. Invest.* **115**, 2192–2201 (2005).
26. Goudriaan, J.R. *et al.* CD36 deficiency in mice impairs lipoprotein lipase-mediated triglyceride clearance. *J. Lipid Res.* **46**, 2175–2181 (2005).
27. Carneheim, C., Nedergaard, J. & Cannon, B. β-adrenergic stimulation of lipoprotein lipase in rat brown adipose tissue during acclimation to cold. *Am. J. Physiol.* **246**, E327–E333 (1984).
28. Hagberg, C.E. *et al.* Vascular endothelial growth factor B controls endothelial fatty acid uptake. *Nature* **464**, 917–921 (2010).
29. Febbraio, M. *et al.* A null mutation in murine CD36 reveals an important role in fatty acid and lipoprotein metabolism. *J. Biol. Chem.* **274**, 19055–19062 (1999).
30. Surwit, R.S. *et al.* Differential effects of fat and sucrose on the development of obesity and diabetes in C57BL/6J and A/J mice. *Metabolism* **44**, 645–651 (1995).
31. Saito, M. *et al.* High incidence of metabolically active brown adipose tissue in healthy adult humans: effects of cold exposure and adiposity. *Diabetes* **58**, 1526–1531 (2009).
32. Zingaretti, M.C. *et al.* The presence of UCP1 demonstrates that metabolically active adipose tissue in the neck of adult humans truly represents brown adipose tissue. *FASEB J.* **23**, 3113–3120 (2009).
33. Vallerand, A.L., Perusse, F. & Bukowiecki, L.J. Cold exposure potentiates the effect of insulin on *in vivo* glucose uptake. *Am. J. Physiol.* **253**, E179–E186 (1987).
34. Skarulis, M.C. *et al.* Thyroid hormone induced brown adipose tissue and amelioration of diabetes in a patient with extreme insulin resistance. *J. Clin. Endocrinol. Metab.* **95**, 256–262 (2010).

ONLINE METHODS

Mice and diets. The Animal Welfare Officers of University Medical Center Hamburg-Eppendorf and Behörde für Soziales, Familie, Gesundheit und Verbraucherschutz Hamburg, Germany approved all experimental procedures. Mice were bred and housed in the animal facility of University Medical Center Hamburg-Eppendorf at 22 °C with *ad libitum* access to standard laboratory chow diet (Ssniff). We used male age-matched (16–22 weeks) *Ldlr*$^{-/-}$, *Apoe*$^{-/-}$ (Jackson Laboratory), *Apoa5*$^{-/-}$ mice (provided by E.M. Rubin and L.A. Pennacchio) as well as LRP1-N2 knock-in (provided by A. Roebroek), *Cd36*$^{-/-}$ (provided by K.J. Moore) and C57BL/6J (Jackson Laboratory) and FVB (Charles River) wild-type mice, which were fasted 4 h before the experiment. Control (22 °C) and cold exposure (4 °C) was performed in single cages for 24 h unless indicated otherwise. To induce insulin resistance and obesity, male C57BL/6J mice were single caged and were at 4 weeks of age fed a diabetogenic high-fat diet[30] *ad libitum* for 16 weeks.

Turnover studies and organ distribution. For turnover studies, anesthetized mice were tail vein–injected with 200 µl radiolabeled TRLs (**Supplementary Methods**). Lipoprotein turnover was determined from 10 µl plasma 0.5, 1, 2, 5 and 15 min after injection. After 15 min, blood was removed by cardiac puncture, the right atrium was opened and the carcass was perfused through the left ventricle with PBS containing 50 U ml^{-1} heparin (Ratiopharm). Then, organs were collected and weighed. For measurement of radioactivity, organs were solubilized in Solvable (PerkinElmer, 0.1 ml per 10 mg organ), 200 µl were counted in scintillation fluid and TRL uptake was calculated as c.p.m. per mg organ. For total organ uptake calculations, we used the estimated organ weights shown in **Supplementary Table 3** (for lean mice) or **Supplementary Table 4** (for obese mice). Oral fat tolerance tests were performed by gavage of 100 µl olive oil with [9,10-^{3}H(N)]-triolein (370 kBq per mouse). To measure lipoprotein production, Triton WR-1339 (Tyloxapol from Sigma; 0.5 mg per g body weight as 10% wt/vol solution in PBS) was injected into the tail vein. Plasma was collected at various time points as indicated in **Supplementary Figures 5** and **6**. For the measurement of hepatic production, 1(3)-^{3}H glycerol (125 kBq per mouse) was injected before Triton WR-1339. Lipids were extracted from plasma samples[35], and ^{3}H-glycerol was incorporated into triglycerides was measured as described above. For chylomicron production, mice received ^{3}H-triolein in olive oil by gavage as described above directly after Triton WR-1339 injection. Intestine-derived radioactivity in plasma was measured as described above. For manipulation of LPL function, tetrahydrolipstatin (Roche, 12.5 mg ml^{-1} DMSO) was diluted to 1.25 mg ml^{-1} in 10% DMSO in PBS. Mice received 200 µl of either 0.25 mg tetrahydrolipstatin, 50 U heparin (Ratiopharm) or 10% vol/vol DMSO in PBS (mock). After 1 min, ^{59}Fe-SPIO- and ^{3}H-triolein-labeled TRLs were injected, and plasma clearance and organ uptake were determined as described above. For postprandial studies, mice were intraperitoneally injected with 0.25 mg tetrahydrolipstatin or mock solution before gavage with 200 µl olive oil. Blood was collected at various time points as indicated in **Figure 3c**, and plasma triglyceride concentrations were determined.

***In vivo* imaging studies.** A detailed description of MRI has been described before[14]. Briefly, all static and dynamic MRI measurements were performed with a clinical 3 Tesla MR scanner (Philips Medical Systems) equipped with a custom-made small animal solenoid coil. The dynamic measurements were based on a gradient-echo sequence (**Supplementary Table 5**). The applied sequence is highly sensitive to susceptibility effects caused by local magnetic field inhomogeneities caused by SPIO-TRLs. DICOM data were processed with ImageJ (http://rsbweb.nih.gov/ij/). For cryoelectron microscopy, SPIO-TRLs were intravenously injected into control or cold wild-type FVB mice. After 30 min, the mice were killed and BAT biopsies were taken and processed for transmission electron microscopy as previously described[36]. Micrographs were obtained with a FEI Eagle 4k charge-coupled device camera and a Tecnai 20 transmission electron microscope operated at 200 kV. For environmental scanning electron microscopy studies of BAT, anesthetized mice were perfused with PBS-heparin as above, and organs were fixed with 2.5% vol/vol glutaraldehyde in PBS, washed and postfixed for 30 min with 1% wt/vol OsO_4 in PBS. For intravital microscopy, interscapular BAT was dissected in anesthetized mice and visualized by a confocal microscope equipped with a resonant scanner (Nikon A1R). QD-labeled TRLs and fluorescent probes were injected via a tail vein catheter, and 15 or 30 confocal images per second were recorded. The acquired data sets were aligned to reduce object movements due to mouse breathing and denoised with a Savitzky-Golay filter in Nikon NIS Elements AR 3.10. Labeling, animations and quicktime-export were done with Adobe After Effects CS4.

Statistical analyses. To assess statistical significance, two-tailed, unpaired Student's *t* test or two-way analysis of variance followed by *post hoc* Bonferroni's test was performed. $P < 0.05$ was considered significant.

Additional methods. Sections describing preparation and labeling of TRL, plasma parameters, RNA extraction and real-time quantitative PCR, endothelial permeability testing and western blotting can be found in the **Supplementary Methods**.

35. Dole, V.P. A relation between non-esterified fatty acids in plasma and the metabolism of glucose. *J. Clin. Invest.* **35**, 150–154 (1956).
36. Hohenberg, H., Tobler, M. & Muller, M. High-pressure freezing of tissue obtained by fine-needle biopsy. *J. Microsc.* **183**, 133–139 (1996).

doi:10.1038/nm.2297